THE JOURNAL OF PHYSICAL CHEMISTRY B

Article

pubs.acs.org/JPCB

Combined EPR and Molecular Modeling Study of PPI Dendrimers Interacting with Copper Ions: Effect of Generation and Maltose Decoration

Sara Furlan,[†] Giovanni La Penna,[‡] Dietmar Appelhans,[§] Michela Cangiotti,[∥] Maria Francesca Ottaviani,*[,∥] and Andrea Danani*[,⊥]

[†]Department of Chemical and Pharmaceutical Sciences, University of Trieste, Via Giorgieri 1, I-34127 Trieste, Italy

[‡]CNR - National Research Council of Italy, ICCOM - Institute for Chemistry of Organometallic Compounds, via Madonna del Piano 10, I-50019 Sesto Fiorentino, Firenze, Italy

[§]LIP - Leibniz-Institut für Polymerforschung e.V., Hohe Straße 6, 01069 Dresden, Germany

[∥]UNIURB - University of Urbino, Department of Earth, Life and Environment Sciences, Crocicchia, I-61029, Urbino, Italy

[⊥]SUPSI - University of Applied Sciences of Southern Switzerland, Department of Innovative Technologies, Galleria 2, CH-6928 Manno, Switzerland

ABSTRACT: Understanding the early onset of neurodegeneration is crucial to deploy specific treatments for patients before the process becomes irreversible. Copper has been proposed as a biomarker for many neurodegenerative disorders, being the ion released by pathologically unfolded proteins involved in many biochemical pathways. Dendrimers are macromolecules that bind metal ions with a large ion/ligand ratio, thus, allowing a massive collection of copper. This work provides structural information, obtained via molecular modeling and EPR, for the binding sites of copper in polypropyleneimine (PPI) dendrimers, especially in the maltose decorated form that has potential applications in diagnosis and therapies for various types of neurodegenerations. The analysis of the EPR spectra showed that, at the lowest Cu concentrations, the results are well supported by the calculations. Moreover, EPR analysis at increasing Cu(II) concentration allowed us to follow the saturation behavior of the interacting sites identified by the modeling study.

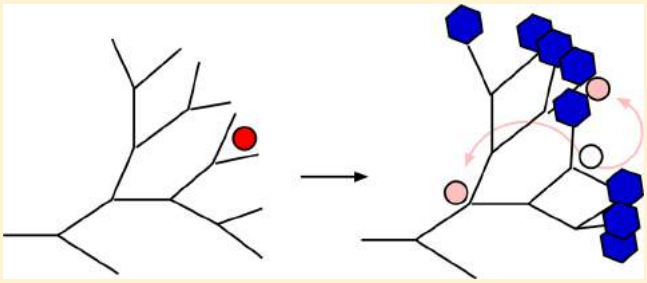

INTRODUCTION

During the early stages of neurodegeneration, a general impairment of the folding ability of cells occurs. Because of this, metal ions, that in normal conditions are properly transported between folded macromolecules, become released by protein carriers and available as free ions in the aqueous cell environment.[1] In these conditions metal ions with catalytic properties (Zn, Cu, Fe) interact with the increasing amount of disordered proteins (some naturally available, some due to the folding impairment), eventually strengthening the level of catalytic activity.[2] A particularly important oxidant pathway that can be activated is the Fenton chemistry of peroxide producing the aggressive hydroxyl radical.[3] This pathway is usually silenced by properly folded macromolecules like peroxidases.

The catalyst widely used by cells for oxidoreductive reactions involving oxygen (reactive oxygen species, ROS) is copper.[4] Indeed, during neurodegeneration the levels of "free" Cu increases and the potential use of Cu as a biomarker has been often proposed.[5−7]

Poly(propyleneimine) (PPI) dendrimers have several properties that are potentially useful in this particular aspect of neurodegeneration, because (i) they can be synthesized with well-defined macromolecular architecture (controlled size, dendrimer generation, decoration with appropriate spacing groups); (ii) terminal and inner chemical groups have well-defined reactivity that, because of the macromolecular architecture, can be combined in a limited space; (iii) they display a large affinity for transition metal ions. Dendrimers are therefore macromolecular nanometer-scale devices with chemical properties which involve transition metal ions and can be modulated by the macromolecular architecture.

Soon after the discovery of dendrimers, it has been recognized that PPI dendrimers behave like macromolecular metal chelating agents. Within the paradigmatic class of PPI, after the investigation of metal binding properties in methanol,[8] this property has been investigated in more details in water by means of MS, UV−vis, and EPR spectroscopies.[9]

Electron paramagnetic resonance (EPR) technique has been found to be very useful to characterize Cu(II)−dendrimer complexation, providing specific information about the

Received: June 2, 2014
Revised: September 23, 2014
Published: September 23, 2014

   dx.doi.org/10.1021/jp505420s | J. Phys. Chem. B 2014, 118, 12098−12111

structure of the complexes, the flexibility of the dendrimers in solution, and to differentiate the internal/external interacting sites of the dendrimers in respect to their availability for ion complexation and trapping.[10−16] Focusing on PPI of generation n up to four (PPI-Gn, hereafter; since the PPI dendrimers are commercially available, we adopted the names of the dendrimers as received from the seller) with no decoration and interacting with Cu at high concentration (more than one Cu ion per dendrimer), these experimental results show that

- The binding of Cu occurs only when the amino terminal groups are available.
- The binding involves mainly three N atoms and the Cu coordination five, when available, is approximately square-pyramidal or trigonal bipyramidal.
- Up to one-half of the available amino terminal groups (for example, 16 over 32 terminal groups in PPI-G4) are Cu-bound when the maximal amount of Cu is bound to PPI.
- The binding of Cu with PPI-Gn does not change significantly with generation n.

This information is almost consistent with the expectation of PPI dendrimers as Cu sponges, with many almost independent Cu-binding sites. However, bare PPI dendrimers are partially cytotoxic, mainly due to the charged amino groups at the external surface.[17] Therefore, they can not be directly used in biological samples and N-termini functionalization (also known as decoration) is required. Conversely, it has been found that the maltose decorated PPI dendrimers are not cytotoxic and may be conveniently used to care cancer and neurodegenerative diseases. When the maltose decoration is present in PPI dendrimers, the features of Cu binding change. In particular, the N_4 coordination of Cu is replaced by square-planar and distorted N_xO_y coordinations, with O atoms belonging to maltose residues or water molecules. This exchange of ligand atoms among N and O atoms is more evident in maltose decorated PPI-G4 (PPI-G4-mal, hereafter) compared to lower generations (n = 2 and 3).[8,9] These results can be followed by the EPR signal of Cu with increasing Cu concentration in the water sample of different complexes.

The structural changes involving PPI-Gn-mal compared to PPI-Gn have not yet been elucidated. In this work, we report the possible structures of PPI-G2 and PPI-G4 bound to a single Cu^{2+} ion and the extent of distortion of the Cu-binding when the PPI-G4 dendrimer is made biocompatible with maltose decoration. These structures are obtained by combining computational models and EPR measurements at different Cu concentration and temperature. In terms of models, the results reported here have been obtained by combining empirical models (Monte Carlo random walks, MCRW hereafter, and classical molecular dynamics, MD hereafter) with short first-principles simulations performed, at the level of density-functional theory for approximating electrons, on selected truncated models. In terms of EPR experiments, the spectral parameters obtained at different concentration and temperature are modeled as sums of different contributions, each obtained with simple geometries. The main features of computational models and EPR measurements are then compared.

METHODS

Molecular Models. Different types of theoretical and computational methods are used to model dendrimers, also in contact with biological macromolecules (see ref 18 for a recent review). Most of the trail blazing simulations reported in the literature deals with poly(amido amine) (PAMAM) dendrimer, studied by means of molecular dynamics simulations (MD) in vacuum performed by Naylor et al. in 1989[19] or by means of Monte Carlo in 1993.[20] Later, several all-atom studies considered more accurate models of PAMAMs using explicit solvent,[21−27] enabling direct comparison with experimentally obtained structural values. For PPI dendrimers, MD simulations about their structure in water are reported in refs 28−30, while we mention here some recent models for PPI combined with other biologically relevant molecules, such as prions,[31] anti-HIV oligodeoxynucleotides,[32] or in the presence of rough models for counterions.[33]

In this work we combine Monte Carlo constructions, simple models of counterions and short molecular dynamics simulations in water to model the bare PPI-G2 and PPI-G4 and their respective maltose decorated form interacting with a single copper cation.

Set-up of Atomic Interactions. We started modeling PPI-G4 and Cu-dendrimer interactions at an empirical level. Since the aim of this work is at placing Cu in different binding sites and modeling the bond fluxionality around Cu models, we used the dummy counterion model for the metal ion.[34,35] The metal ion is a unique Lennard-Jones site with a number of electrostatic hooks displaced around the center. These hooks (with the Du atom name assigned, see Table 1) are, in this case, 6 positive point charges 2/6, placed at the vertices of an octahedron. This model decreases the overestimate of the electrostatic interactions that is a usual effect when the ion is assumed a single +2 point charge.

Table 1. Point Charges q Assigned to PPI-G4 Atoms[a]

atom	q
N (G0-G3)	−0.9
C (α to N)	+0.1
H (α to N)	+0.1
N (G4)	−0.94
HN (G4)	+0.47
Cu	0.0
Du	+1/3
OW (TIP3P)	−0.834
HW (TIP3P)	+0.417

[a]Those not reported are taken from the PARM94 AMBER force-field for Lys residues.[36] The labels Gi indicate the branches in PPI-G4, where G4 is the terminal amino group and G0 is the N atom in the dendrimer core. TIP3P indicates the water model adopted in this work.[37].

The force-field parameters for PPI-G4 atoms are mostly those of the Lys side chain in the PARM94 AMBER force-field.[36] In order to balance interactions between the dummy counterion and possible ligand atoms (N atoms in amino groups of PPI-G4 and O in water molecules modeled as TIP3P sites),[37] a slightly modified charge distribution has been adopted (Table 1) for N atoms in the dendrimer. Since Cu competes with protons for binding amino groups in the dendrimer, we assume none of the amino groups protonated.

In order to model interactions with the maltose decoration, the recent CHARMM36 force-field was adopted for maltose.[38] The parameters for the reduced glucose monomer linking the amino group of PPI-G4, has been transferred from similar groups in the CHARMM36 force-field.

dx.doi.org/10.1021/jp505420s | J. Phys. Chem. B 2014, 118, 12098−12111

Table 2. Dendrimer Parameters for Eight Trajectories of the PPI-G4 Model[a]

trajectory	R_g	L_x	L_y	L_z	b	K^2
0	11.7 (2)	43.70	46.70	41.40	−25 (8)	0.05 (2)
	11.9 (2)	44.25 (6)	47.29 (6)	41.92 (5)	−34 (5)	0.08 (2)
	11.2 (4)	44.25 (6)	47.29 (7)	41.93 (6)	−27 (5)	0.09 (2)
	10.6 (2)	44.26 (6)	47.30 (7)	41.93 (6)	−23 (4)	0.06 (2)
	10.3 (1)	44.26 (6)	47.30 (6)	41.93 (6)	−23 (2)	0.06 (1)
	10.3 (2)	44.26 (6)	47.30 (7)	41.93 (6)	−20 (3)	0.06 (1)
4	12.0 (3)	43.70	46.70	41.40	−40 (5)	0.15 (2)
	11.3 (2)	44.25 (6)	47.28 (6)	41.92 (6)	−27 (5)	0.10 (2)
	11.1 (4)	44.25 (6)	47.29 (7)	41.92 (6)	−30 (7)	0.10 (4)
	10.8 (2)	44.26 (6)	47.29 (7)	41.93 (6)	−27 (3)	0.10 (2)
	10.5 (2)	44.24 (6)	47.28 (7)	41.92 (6)	−24 (3)	0.08 (2)
	10.2 (2)	44.25 (6)	47.29 (7)	41.92 (6)	−21 (5)	0.07 (3)
8	11.7 (2)	43.70	46.70	41.40	−27 (4)	0.66 (1)
	11.7 (2)	44.24 (6)	47.28 (7)	41.91 (6)	−40 (10)	0.14 (6)
	12.1 (3)	44.25 (6)	47.28 (7)	41.92 (6)	−56 (5)	0.20 (2)
	11.6 (3)	44.25 (6)	47.29 (7)	41.92 (6)	−51 (4)	0.15 (1)
	11.1 (1)	44.25 (6)	47.28 (7)	41.92 (6)	−45 (3)	0.13 (1)
	10.8 (2)	44.24 (6)	47.28 (6)	41.91 (6)	−36 (3)	0.12 (1)
12	11.9 (2)	43.70	46.70	41.40	−37 (4)	0.13 (2)
	11.3 (3)	44.24 (6)	47.28 (6)	41.91 (5)	−37 (5)	0.13 (3)
	11.4 (1)	44.25 (6)	47.29 (7)	41.92 (6)	−38 (4)	0.15 (4)
	11.1 (2)	44.25 (6)	47.29 (6)	41.92 (6)	−37 (2)	0.21 (2)
	10.9 (3)	44.25 (6)	47.28 (7)	41.92 (6)	−37 (2)	0.17 (4)
	10.5 (1)	44.24 (6)	47.28 (7)	41.92 (6)	−33 (2)	0.13 (2)
16	11.4 (4)	43.70	46.70	41.40	−28 (5)	0.05 (1)
	11.1 (2)	44.25 (6)	47.29 (7)	41.92 (6)	−29 (4)	0.10 (4)
	10.8 (2)	44.25 (6)	47.29 (7)	41.92 (6)	−26 (3)	0.12 (2)
	10.8 (2)	44.25 (6)	47.29 (7)	41.92 (6)	−31 (4)	0.14 (4)
	10.2 (2)	44.25 (6)	47.29 (7)	41.92 (6)	−29 (5)	0.13 (3)
	10.2 (2)	44.26 (6)	47.29 (7)	41.93 (6)	−25 (2)	0.14 (3)
20	11.8 (2)	43.70	46.70	41.40	−48 (3)	0.14 (2)
	10.7 (3)	44.25 (6)	47.29 (7)	41.92 (6)	−31 (4)	0.14 (2)
	10.3 (2)	44.25 (7)	47.29 (7)	41.92 (6)	−27 (3)	0.14 (3)
	10.3 (2)	44.25 (6)	47.29 (7)	41.92 (6)	−26 (3)	0.15 (3)
	11.0 (2)	44.26 (6)	47.30 (7)	41.93 (6)	−32 (4)	0.18 (2)
	11.2 (2)	44.25 (6)	47.29 (6)	41.92 (6)	−37 (3)	0.21 (2)
24	11.9 (3)	43.70	46.70	41.40	−34 (4)	0.09 (2)
	12.6 (4)	44.24 (6)	47.28 (7)	41.92 (6)	−52 (9)	0.14 (2)
	11.7 (4)	44.25 (6)	47.28 (7)	41.92 (6)	−43 (7)	0.11 (2)
	12.1 (2)	44.25 (6)	47.28 (7)	41.92 (6)	−52 (5)	0.16 (3)
	12.2 (2)	44.25 (6)	47.29 (7)	41.92 (6)	−45 (5)	0.18 (4)
	12.0 (3)	44.25 (6)	47.29 (7)	41.92 (6)	−40 (4)	0.23 (3)
28	12.5 (3)	43.70	46.70	41.40	−44 (4)	0.12 (2)
	12.1 (2)	44.25 (6)	47.29 (7)	41.92 (6)	−38 (4)	0.12 (3)
	11.7 (3)	44.25 (6)	47.29 (7)	41.92 (6)	−42 (5)	0.15 (2)
	11.7 (2)	44.25 (6)	47.29 (7)	41.92 (6)	−38 (5)	0.17 (4)
	10.8 (5)	44.26 (6)	47.30 (7)	41.93 (6)	−35 (5)	0.14 (2)
	10.2 (1)	44.26 (6)	47.30 (7)	41.93 (6)	−30 (2)	0.15 (2)

[a]Averages computed over the NVT trajectories (first row for each trajectory) are compared with 5 separated 1 ns averages computed along the 5 ns NPT trajectories (rows 2-6). R_g is gyration radius (Å), L_α ($\alpha = x, y, z$) are the sides of the orthorhombic simulation cell (Å), b and K^2 are the shape anisotropy parameters (see Methods). Computed root-mean square errors are reported on the last digit of the respective average within brackets. The time-range (t in ps) used for averaging the NVT trajectories is reported in Table 3.

Set-up of Dendrimer Initial Structures. The initial PPI-G4 configuration was built in an *all-trans* configuration for the X−CH_2−CH_2−X dihedral angles, while the geometry of the amino groups was in identical *gauche*± states in all the branches. The atomic overlaps that occur in such initial regular configuration were removed with a Monte Carlo random-walk (MCRW) approach applied to all the dihedral angles involving nonhydrogen atoms,[39,40] with no Cu ions and no water solvent molecules. The Monte Carlo moves were accepted or rejected according to the Metropolis test performed with random inverse temperature within infinity ($T \sim 0$) and 0 ($T = 10000$ K). This procedure avoids configurations with overlapping or entagled chains. The statistics is a rough estimate of the density of states in the sampled dihedral space and in the vacuum,

dx.doi.org/10.1021/jp505420s | J. Phys. Chem. B 2014, 118, 12098−12111

accounting mainly for excluded volume effects due to the branched dendrimer topology. The sampled dihedral angles are randomly changed in the $[0,2\pi]$ range. The acceptance ratio in the MCRW was within 1/3 and 1/2, with a collective move assumed when all the dihedral angles are attempted to move.

Inserting Copper Ions into PPI-G4 Models. A set of 10000 configurations of PPI-G4 was collected with the MCRW. The collected configurations were analyzed in order to find random sites available for Cu coordination. For every pair of N atoms at a distance smaller than 6 Å, a potential Cu atom is placed midway. Then, the number of N atoms at a distance lower than 3 Å from this added Cu site are counted. The coordination number, CN, is defined as

$$\mathrm{CN} = \sum_i s_i \tag{1}$$

$$s_i = 1 \quad \text{if} \quad r_i \leq 0$$

$$s_i = \frac{1 - (r_i/r_{i,0})^6}{1 - (r_i/r_{i,0})^{12}} \quad \text{if} \quad r_i > 0$$

$$r_i = |r_i| - r(\mathrm{Cu})| - d_0 \tag{2}$$

Such definition of coordination number CN as a continuous variable has been derived by a similar definition provided for hydrogen bonds.[41] The index i runs over all the N in the PPI-G4 ligand. The parameters $r_{i,0}$ and d_0 were 0.5 and 2.0 Å, respectively, according to an expected Cu−N bonding distance in the range 2−2.5 Å.

This analysis provided no coordination (CN = 0) of Cu to N(G0) and N(G2) atoms, indicating with Gn within brackets the chain terminus belonging to the n-generated branch. A number of 80 configurations over 10000 displayed a CN ≥ 3.5 involving N(G3) and N(G4) atoms. These data show that the possible accommodation of Cu within branches close to the dendrimer core (G0, G1, and G2) is, in the given model, never possible by chance. Though, a structural rearrangement assisting Cu binding to dendrimer core is not excluded as a possible alternative.

Refining Models with All-Atoms MD Simulations. A set of 32 independent configurations was chosen among the 80 Cu-bound configurations found within the MCRW trajectory, for performing all-atoms MD simulations, including an explicit model for the water solvent environment. Each of the 32 configurations was merged into an orthorhombic cell with cell axes of 4.37, 4.67, and 4.14 nm, respectively. An identical number of 2697 water molecules was added to every configuration, by modulating the minimal Ow−X distance within 0.12 and 0.15 nm, with X being any atom in the Cu-dendrimer complex and Ow being the O atom of any water molecule. The smooth particle-mesh Ewald technique was used for long-range electrostatics.[42] The distance cutoff for non-bonding interactions was 1.1 nm, with a sigmoidal switching starting at 1 nm. The time-step was 0.5 fs. The NAMD 2.9 program was used for all the empirical simulations.[43] The RATTLE algorithm was used for constraining all the bonds involving H atoms to their respective equilibrium distance.[44]

Each of the 32 configurations was simulated separately in the NVT statistical ensemble by using a weak coupling with an external bath.[45] The relaxation time for the temperature (τ_T in reference above) was 5 ps. The close by minimal energy was first searched as a function of water and Cu positions. Then, the close by minimal energy as a function of all the coordinates was reached and the system was heated up to T = 300 K in two stages of T = 100 and 200 K, of 10 ps each, with a stochastic thermostat.[45] Then, 1 ns of simulation with the same thermostat at T = 300 K was collected for all the 32 trajectories.

A subset of the 32 MD trajectories for PPI-G4 was chosen to check the effects of extending the time length of each MD trajectory and the possible deviations between trajectories due to the different pressure associated with each initial sample. After 1 ns of equilibration in the canonical (NVT) statistical ensemble, 8 trajectories were extended for 5 ns in the isothermal and isobaric (NPT) statistical ensemble, by weakly coupling the system to an external bath at the pressure of 1 bar, with the isothermal compressibility β of bulk water at room conditions (4.57×10^{-5} bar^{-1}) and the relaxation time (τ_P in ref 45) of 0.1 ps.

The comparison between the short NVT trajectories and five different 1 ns subaverages computed during the time-range of 5 ns in the NPT extensions, is reported in Table 2. The coordination number (CN) of Cu is constant with the change of boundary conditions (data not shown). The relaxation of the volume provides an expansion of about 0.5 Å at each side of the simulation cell for all eight samples, with no significant change after 1 ns of NPT simulation. This slight reduction of water density around the dendrimer provides, with the exception of trajectory 24, the condition for a slight compaction of the dendrimer, as witnessed by the decrease of gyration radius (R_g). This occurs because of the extrusion of water molecules from the macromolecule and the consistent partial hydrophobic collapse of the solute macromolecule. The collapse is almost isotropic, since the discoidal (see comments about b in Results) shape of the dendrimer is not significantly changed by the volume expansion.

The experimental radius of gyration measured for the PPI-G4 dendrimer in water solution (with no Cu added) is 11.6 Å (see Results).[46] Within the short NVT simulations performed by us for the PPI-G4 dendrimer, we do not notice significant differences due to the 1:1 Cu addition to the dendrimer (see Results). Therefore, the slight collapse of the dendrimer at the constant external pressure of 1 bar is likely an artifact of the force-field used for the simulation, and we prefer to analyze the configurations more consistent with the available experimental data. The short NVT simulations were then extended to all the 32 samples built at constant density and to the other models (including those with the maltose decoration).

Adding the Maltose Decoration to PPI-G4-Cu. At the end of the PPI-G4 simulation, for each of the 32 final configurations, the water molecules were removed and maltose residues were linked to each of the N-terminal groups, including those bound to Cu. The bond between C1 and the oxygen atom in the pyranose ring (denoted O5) in each of the reducing monomers was removed and replaced with a C1−H1 bond. On the other side, the O5 atom is bound to an added H atom. The maltose decoration was then settled for the closeby energy minimum, and atomic overlaps were smoothly removed by slowly increasing the extent of repulsive interactions. The energy of the total system was then minimized. These models will be indicated as PPI-G4-mal-Cu, hereafter.

The 32 PPI-G4-mal-Cu molecules were merged into identical cubic cells with cell axis of 5.7 nm and the simulation box was filled with 5439 water molecules, by a procedure identical of that adopted for the PPI-G4-Cu configurations. After stages of energy minimization and three stages of 10 ps each of heating up to T = 100, 200, and 300 K, respectively, 1

dx.doi.org/10.1021/jp505420s | J. Phys. Chem. B 2014, 118, 12098−12111

ns of trajectory in the NVT statistical ensemble was collected for each of the 32 initial configurations.

Settling Final Configurations in DFT Model. A selected number of final configurations in the classical trajectories described above was selected to refine the interactions between Cu, the dendrimer and the portion of water molecules interacting with both the species. Segments of the dendrimer were cut away from the macromolecule in order to keep the systems within a reasonable size (about 500 atoms including water molecules). For comparisons, the same systems were also simulated at low temperature, keeping only the initially Cu-bound water molecules and removing the solvent water molecules. The goal of these models is to check if the collected empirical models for Cu coordination to PPI-G4-Cu and PPI-G4-mal-Cu are too far away from more realistic descriptions of the electronic structure, especially in the proximity of the Cu ions.

Molecular dynamics simulations within the extended Lagrangian formalism (also known as Car−Parrinello method[47,48] and indicated with CP-MD, hereafter) were performed on the selected systems. The parallel version of the Quantum-Espresso package,[49] which incorporates Vanderbilt ultrasoft pseudopotentials[50] and the PBE exchange-correlation functional,[51] was used in all CP-MD simulations. Electronic wave functions were expanded in plane waves up to an energy cutoff of 25 Ry, while a 250 Ry cutoff was used for the expansion of the augmented charge density in the proximity of the atoms, as required in the ultrasoft pseudopotential scheme.

To minimize finite volume effects, periodic boundary conditions were imposed to the system. Each initial model for the Cu−peptide complex was inserted in a supercell with cell dimensions chosen to maximize the separation between nearest-neighbor replicas of the system so as to have minimal spurious self-interactions, but keeping the system size manageable. All the CP-MD calculations were performed under spin-restricted conditions. Simulations have been carried out according to the following general protocol consisting of the three sequential steps: (1) minimization of electronic energy with fixed atomic positions; (2) minimization of total energy as a function of both atomic and electronic degrees of freedom; (3) a series of sequential CP-MD simulations of 0.1−0.5 ps, each at fixed increasing atomic temperatures from 50 to 300 K, with temperature held fixed by a Nosé−Hoover thermostat.[52]

The energy minimization of steps 1−2 were performed via damped CP-MD, with a damping frequency for all the degrees of freedom of $1/(10\delta t)$ and with δt the time-step of 0.12 fs used for all the CP-MD simulations in this work. The number of minimization time-steps was in the range of 1000, depending on the system size. Steps 1−2 are required to begin the following $T > 0$ CP-MD simulation with atomic velocities of low magnitude: in all cases the maximal initial velocity for any atom was smaller than 0.003 Å/fs. The thermalization procedure described in step 3 is necessary to slowly reach the target temperature, thus avoiding temperature oscillations that may affect in an uncontrolled way the approach of electrons to their ground state. The velocity-Verlet algorithm for integrating the CP-equations of motion was used with a time step of 0.12 fs.[53]

The CP-MD simulations for the nonsolvated systems at T = 50 K were performed for 0.6 ps for five representative selected models (3 within PPI-G4 and 2 within PPI-G4-mal). These simulations are the local minimization of the initial systems. The final configurations were analyzed in order to better assess the Cu coordination exploited at the empirical level by MD simulations. In some cases we performed simulations of the same systems in small samples of explicit water molecules, carrying the systems to the temperature T of 300 K in one step (T = 150 K) starting from the same initial solute configuration used for the simulation in the vacuum at T = 50 K.

Materials and Sample Preparation. PPI-G2 and PPI-G4 dendrimers were supplied by SyMO-Chem (Eindhoven, Netherland). The maltose decorated dendrimers were synthesized according to published procedures.[54] The dendrimers were dissolved in Millipore doubly distilled water resulting in a final surface group concentration of 0.1 M. Cupric nitrate hydrate ($Cu(NO_3)_2{\cdot}2.5H_2O$, Sigma- Aldrich, ACS reagent 98%) was also dissolved in Millipore doubly distilled water to obtain a final concentration, in the mixture with the dendrimers, from 0.0025 to 0.5 M. After different equilibration times (from freshly prepared to 1 day aging), 100 μL of the dendrimer-copper solution was inserted in an EPR tube (1 mm internal diameter).

EPR Measurements. EPR spectra were recorded by means of an EMX-Bruker spectrometer operating at X band (9.5 GHz) and interfaced with a PC (software from Bruker for handling and analysis of the EPR spectra). The temperature was controlled with a Bruker ST3000 variable-temperature assembly cooled with liquid nitrogen. The EPR spectra were recorded for the different samples at 298 and 150 K. In all cases, we controlled the reproducibility of the results by repeating the EPR analysis (three times) in the same experimental conditions for each sample.

Simulation of EPR Spectra. The EPR spectra at both room and low temperature were computed by using the procedure reported by Budil et al.,[55] which was created for computing nitroxide radical spectra. But this procedure was successfully applied to the simulation of Cu(II) spectra too. However, we compared the simulations with the Budil et al. procedure with other computational methods, such as (a) the CU23 program kindly provided by Prof. Romanelli (University of Florence, Italy); (b) the Bruker WIN-EPR SimFonia Software Version 1.25; and (c) the program EasySpin 4.5.1, using MATLAB 7.5. We considered satisfactory a spectral simulation that produces the best fitting between the experimental and the simulated spectra. The main parameters obtained from spectral simulation at both low and room temperatures were (a) the g_{ii} components (accuracy in the third decimal digit, on the basis of the simulation itself) for the coupling between the electron spin and the magnetic field; (b) the A_{ii} components (accuracy of about ±0.01 G) for the coupling between the electron spin and the nuclear spin (I(Cu) = 3/2); (c) the line widths W_i of the x, y, and z lines (accuracy ±0.01 G); and (d) the correlation time for the rotational diffusion motion of the ions and their complexes, τ, which is related to the flexibility of the dendrimer structure in the region where Cu^{2+} is located. The magnetic parameters g_{ii} and A_{ii} were first directly measured in the spectra by field calibration with the DPPH radical (g = 2.0036), and then we used these parameters as starting values for the spectra simulation, changing them until the best fitting between the experimental and the simulated spectra was obtained.

In several cases the spectra were constituted by two or three components due to different coordination and geometries of Cu(II)-dendrimer complexes. The subtraction between the spectra in different experimental conditions allowed extraction

of the spectral components constituting the overall EPR spectra. The different components were computed separately. The subtraction procedure also allowed us to calculate, by double integration of each component, the relative percentages of the different components, with an accuracy of 2%.

We found that the simulations of the observed EPR signals provided a useful means of estimating the spectral parameters but did not necessarily produce unique fits. However, we trusted the parameters which provided best fitting of a series of spectra in similar experimental conditions.

The magnetic parameters extracted from the simulation were then compared with equivalent parameters found in the literature.[9,56−61] This allowed us to assign each spectral component to a copper coordination and to identify the structure and coordination sites of the dendrimers.

Analysis of Molecular Models. The coordination number of Cu is analyzed via the CN parameter described above.

The gyration radius (R_g) is defined as the root-mean square distance between all the dendrimer atoms and the geometrical center of the same set of atoms. As usually done in polymer physics, no mass-weight is applied. The shape of the PPI dendrimer is analyzed via the three eigenvalues of the rank-2 gyration tensor $\mathbf{S}$:[62]

$$\mathbf{S}_{\alpha,\beta} = \frac{1}{N}\sum_{i=1}^{N} \mathbf{r}_{i,\alpha}\mathbf{r}_{i,\beta} \tag{3}$$

with i running over the N atoms, and α and β running over the three Cartesian components of atomic positions $\mathbf{r}$, these latter with respect to the center of mass in the selected molecule. The ranking of $\mathbf{S}$ eigenvalues allows the identification of the shape as oblate (discoidal) or prolate (cylindrical) ellipsoid. The asphericity b and the relative shape anisotropy K^2 are used to quantify the shape anisotropy:

$$b = \lambda_3 - \frac{1}{2}(\lambda_1 + \lambda_2) \tag{4}$$

$$K^2 = 1 - 3\frac{\lambda_1\lambda_2 + \lambda_2\lambda_3 + \lambda_3\lambda_1}{(\lambda_1 + \lambda_2 + \lambda_3)^2} \tag{5}$$

with λ the eigenvalues of $\mathbf{S}$. The above parameters are averaged over the analyzed configurations in the trajectories.

The radial distribution function of two sites ($g(r)$) is defined, as usual, as the ratio between the measured probability of finding the distance between two sites within a given range to the probability in the uniform ideal gas with the same density of the addressed sites.

RESULTS

Computational Models. *Dendrimer Structure.* At first the time evolution of selected parameters describing the global structure of the macromolecules was analyzed.

The gyration radius for the different models has been analyzed along with time (data not shown here). This observation leads to chose different final time windows for averaging over all the independent samples simulated. Table 3 summarizes these values and the resulting averages for the gyration radius compared with available experimental values when no Cu is added to the dendrimers.[46] These data show that the effect of the addition of a single Cu ion to the dendrimer has a small effect on the size of the macromolecule. Despite the basic model assumed for the atomic interactions, the size of the macromolecule is, for both the simulated

Table 3. Gyration Radius R_g in Å of PPI Models, Compared with Available Experimental Values (Exp.) Obtained by Small Angle X-ray Scattering with No Cu[46a]

model	N_{repl}	t/t_{tot}	N_c	R_g (Å)	exp.
PPI-G4 (no Cu)	16	200/400	80	11.2 (0.5)	11.6
PPI-G2	8	500/1000	100	6.6 (0.4)	6.9
PPI-G4	32	370/670	74	11.6 (0.4)	11.6
PPI-G2-mal	8	500/1000	100	6.5 (0.5)	
PPI-G4-mal	32	370/990	74	12.1 (0.3)	

[a]The radius is computed discarding Cu and decoration from the sum. Computed root-mean square errors are reported within brackets. The first columns report the number of replica (N_{repl}), the time-range (t in ps) over the total simulated time for and the number of configurations (N_c) used for averaging (for each replica).

generations, in agreement with the experimental values. The effect of the addition of the maltose decoration is larger than the addition of Cu binding, especially for generation 4.

A more detailed analysis helps in understanding the change of shape of dendrimers when the decoration is added. The ranking of the eigenvalues of the gyration tensor for the two PPI-Gn models simulated, shows that the PPI structures can be assimilated, in all cases, to oblate ellipsoids. According to this observation, the asphericity b parameter (see Methods) is in the negative range, with the gyration radius $R_g \sim 2(-b)^{(1/2)}$. The comparison of shape anisotropy parameters (Figure 1 for PPI-

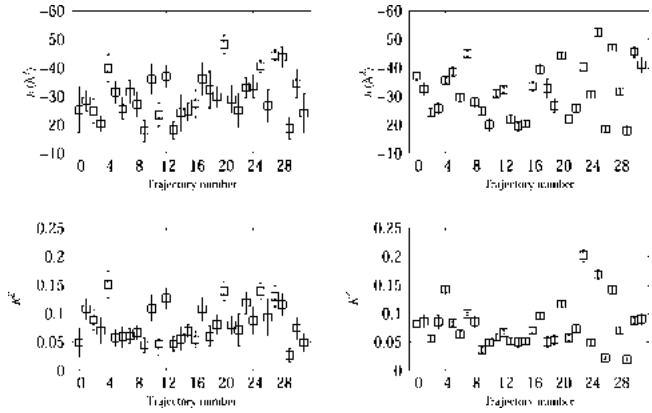

Figure 1. Asphericity (b, top) and shape anisotropy (K^2, bottom; see Methods) averaged over the last 370 ps of the different trajectories: PPI-G4 (left) and PPI-G4 decorated with maltose (right). The root-mean square errors are reported as error bars.

G4) shows that the maltose decoration has a moderate effect on the discoidal average structures. It can be noticed that the major effect of maltose decoration is the freezing of the structures in one of the shapes accessible with no decoration. This effect is displayed by the smaller fluctuations (error bars) for each plotted value when decoration is included in the model. In some of the trajectories, the b parameter decreases significantly when maltose residues are present (trajectory 25).

The time evolution of such parameters (data not shown) indicate that the approximate convergence of the data is reached in the same time-scales observed for the gyration radius (see Table 3). The effect of glicosylation on the PPI dendrimer observed here is similar to that observed in proteins. For instance, in the case of SH3 domain protein, glicosylation provides the loss of plasticity for the protein structure, by

dx.doi.org/10.1021/jp505420s | J. Phys. Chem. B 2014, 118, 12098−12111

increasing the energy barrier between the folded and unfolded states.[63]

Statistics of Cu Coordination Modes. Since we used an octahedral dummy counterion model for Cu^{2+}, the number of ligand atoms around Cu is always 6. In the following, we exclude from the coordination count the water molecules and we concentrate on the interactions between Cu and dendrimer atoms.

The graphical inspection of the Cu-bound configurations built by the random insertion approach (see Methods) showed that one-half of the configurations built for PPI-G4-Cu are consistent with the chelating structure proposed on the basis of EPR spectra in the early studies of PPI-G4-Cu.[8] In Table 4 the topologies of the Cu-binding sites selected for further MD simulations are summarized. Among the configurations built with the MCRW, we selected the configurations with CN > 3 and the first 32 and 8 configurations for PPI-G4 and PPI-G2, respectively, were analyzed in more detail. The fractions reported in the table measure roughly the different propensities for hosting candidate Cu-binding sites in different dendrimer regions, according to excluded volume considerations for the PPI-G*n* dendrimer. From the analysis reported in Table 4, the most likely binding site in PPI-G4 is within the N-terminus of each branch (13 over 32 configurations), consistently with the model proposed in ref 8 and with the existence of 16 independent metal-binding sites, that is, one for each branch at G3 nodes. A few N_4 binding sites (2 over 32, class A) display two different branches binding the same Cu ion. While 17 configurations over 32 bind the Cu ion with at least 3 N atoms (classes A–C), 15 configurations display less than 3 N atoms binding Cu (classes D–F). None of the candidate sites involve the inner amino groups N(G2), N(G1), and N(G0).

After the MD simulation in explicit water, each trajectory tends to keep its own initially built coordination and only a few trajectories undergo a change in Cu coordination because of the structural relaxation in the explicit solvent. In Figure 2, left panel, the coordination number-averaged over the last 0.37 ns are reported for each trajectory. Most of the sites are of type N_3O (14 over 32), resulting from the water binding to the initial N_3 sites. In Figure 3, a representative structure of type N_3O is displayed. Also the 2 N_4 sites are kept for the whole simulations of the respective initial configurations. In summary, the initially built configurations well adapt to the solvation environment modeled with explicit TIP3P water molecules and to thermal fluctuations at room conditions. In the case of PPI-G4, the 5 ns long extension (see Methods) of 1/4 of the trajectories (trajectory numbers 0, 4, 8, 12, 16, 20, 24, and 28) shows a constant coordination number, despite a slow compaction of the dendrimer. These data, taken together, show that once an initial Cu coordination is assembled, it is rather insensitive to thermal fluctuations of the dendrimer structure.

The statistics reported above for PPI-G4 is slightly different for PPI-G2. The initial Cu coordination is in 3 cases over 8 the configuration with Cu chelated within the N terminus of a dendrimer branch, but in many cases (4 over 8) the Cu ion access the dendrimer core (N(G0)). This latter is the most significant difference compared to PPI-G4, where the N(G2)

Table 4. Summary of Types of Cu Coordination Selected within MCRW of the PPI-G2 and PPI-G4 Models[a]

label	coordination	topology	number of replica
G2			(/8)
A	N_3···N	N(G2)-N(G1)-N(G2)···N(G2)	3
B	N_3···N	N(G0)-N(G1)-N(G2)···N(G2)	4
C	N_2···N_2	N(G1)-N(G2)···N(G1)-N(G2)	1
G4			(/32)
A	N_3···N	N(G4)-N(G3)-N(G4)···N(G4)	2
B	N_3	N(G4)-N(G3)-N(G4)	13
C	N_2···N	N(G3)-N(G4)···N(G4)	2
D	N_2	N(G3)-N(G4)	7
E	N···N	N(G4)···N(G4)	5
F	N	N(G4)	3

[a]The selection is performed on the basis of geometrical constraints (see Methods). The numbers indicate the number of replica with the indicated coordination. The total number of replica for G2 and G4 is, respectively, 8 and 32.

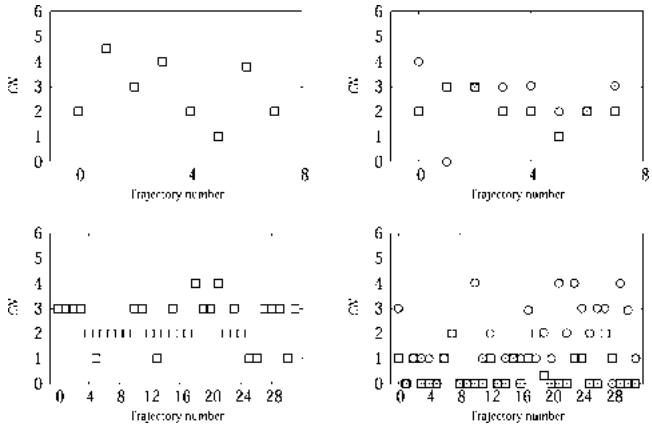

Figure 2. Coordination number of Cu (CN, see Methods) averaged over the last half of the different trajectories (370 ps for PPI-G4 and 500 ps for PPI-G2): PPI-G2 (top left), PPI-G2 decorated (top right), PPI-G4 (bottom left), and PPI-G4 decorated with maltose (bottom right). Squares are for Cu–N pairs (Cu–N(G3,G4) for PPI-G4), circles for Cu–O(mal) pairs.

Figure 3. Representative configuration (trajectory 0 after 0.67 ns) of PPI-G4 with the N3 coordination. Water molecules and H atoms are not displayed.

atoms are never bound to Cu (Table 4). After equilibration in explicit water, two of the N atoms involved in the initial N_4 coordinations are kept bound to Cu in 7 cases over 8, while in 3 of these 7 cases the N_4 coordination is kept almost unchanged.

After the construction of the maltose decoration and the following equilibration of the macromolecules, the behavior of the Cu coordination changes with more significantly with the generation for PPI-mal compared to PPI. In PPI-G2-mal the initial Cu-binding sites are only slightly changed by maltose. Even if none of the N_4 coordination is kept, only in 1 case over 8 the number of N atoms binding Cu reduces to 1 (trajectory 5 in Figure 2, top-right). By observing each of the final configurations of the MD trajectories (data not shown), it can be observed that the O atoms of maltose can easily enter into che coordination sphere of Cu in PPI-G2, without extracting the ion from the initial sites.

On the other hand, in PPI-G4-mal most of the Cu ions are displaced by N binding (Figure 2, bottom-right panel). Coordination number CN $\geq$ 3 involving O maltose atoms is displayed in 10 trajectories over 32. In five of these cases, all of the involved Cu ligands are O atoms of the maltose decoration and N atoms of the N-termini are not binding Cu. Five trajectories over 32 display the extraction of Cu from ligand atoms belonging to the dendrimer into water (the points with circles and squares at CN = 0). In all the other cases, both N(PPI) and O(maltose) bind Cu together. Noticeably, in one case Cu binds N(G0) (i.e., the dendrimer core). Again, this latter condition was never fulfilled for PPI-G4-Cu.

To understand which interaction due to the maltose decoration contributes to the movement of the Cu ion in PPI-G4-mal, we measured the intramolecular hydrogen bonds involving hydroxyl groups of the glucose residues. In both cases (PPI-G2-mal and PPI-G4-mal) the population of hydrogen bonds was low: in PPI-G2-mal only 4 groups over 64 have a hydrogen bond percentage larger than 10%; in PPI-G4-mal this fraction is even lower, 6 over 256 groups. This means that there is not an increase in the number of interactions involving a possible hydrogen bond network within glucose residues in the decoration.

There are significant changes between PPI-G2-mal and PPI-G4-mal in the extent of dendrimer–water interactions. These interactions are different among the different replica. In Figure 4, we show the $g(r)$ function for pairs involving dendrimer core atoms and O of water molecules and for three different cases in PPI-G4-mal. The thick line is the result for trajectory 0, where the Cu ion is embedded in the hydroxyl groups of the decoration. The dashed line is for trajectory 4, where Cu is in the N_2O_2 coordination (with O belonging to water molecules). The thin line is for trajectory 7, where Cu binds the dendrimer core, N(G0). It can be noticed that in this latter case a significant increase in core solvation occurs, showing that when the Cu ion moves toward the core it drags water molecules with it. This effect is rather unexpected, because the hydrophilic nature of the maltose decoration is expected to keep water around the outer shell of the PPI scaffold.

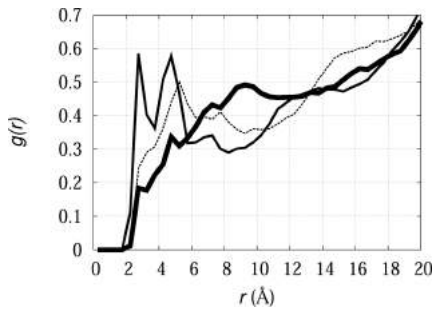

Figure 4. Radial distribution function ($g(r)$) for pairs involving dendrimer core atoms and O of water molecules in PPI-G4-mal: trajectory 0 (thick line); trajectory 4 (dashed line); trajectory 7 (thin line).

To summarize the different behavior of PPI-G2 and PPI-G4 when the maltose decoration is added, the radial distribution function of N PPI atoms is compared among the four simulated models in Figure 5. While the location of the peaks is unchanged in PPI-G2, in PPI-G4 the peak at 3 Å disappears when maltose is added (thin curve in right panel). This is the indication of the opening of the N-termini in PPI-G4-mal, an effect that does not occur in PPI-G2-mal. Since the chemical changes occurred at the N PPI termini because of the formation of the N-mal bonds are the same, the separation of N terminal groups in PPI-G4-mal is due to the structure adopted by the maltose fragments at the density available for generation 4. This structure dominates over the dendrimer mechanics, thus, ejecting Cu toward other binding sites, mostly within the maltose decoration.

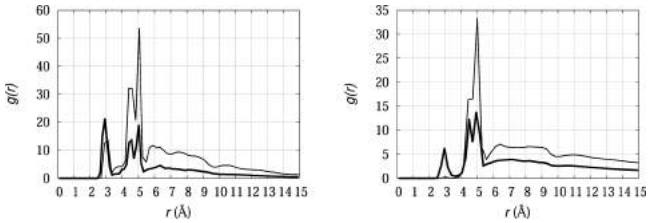

Figure 5. Radial distribution function ($g(r)$) for N–N pairs in PPI-G2 (left, thick curve), PPI-G2 decorated (left, thin curve), PPI-G4 (right, thick curve), and PPI-G4 decorated (right, thin curve).

Cu Binding Sites in DFT Models. For several configurations, selected as final points in the trajectories of the empirical PPI-G4 models, calculations at the level of density-functional theory were performed, in order to better describe the interactions between the Cu ion and the dendrimer macromolecule. Starting from the six-coordinated Cu models, short simulations (0.6 ps) at the temperature T = 50 K in the vacuum were performed, within the extended Lagrangian (Car–Parrinello) scheme (see Methods). These simulations allow the settling of the empirical model in the DFT model, thus, decreasing the Cu coordination number toward the closest value accessible to the initial empirical model.

In all the simulated configurations, the backbone atoms of the molecular fragments do not change significantly their position, while the Cu atom and the water molecules initially bound to Cu change their positions according to the electron density providing the minimal total energy to the truncated systems (see Methods for details). In most of the cases, some of the water molecules initially bound to Cu move far from Cu, providing a lower Cu coordination. Nevertheless, these limited structural changes preserve the location of dendrimer ligand atoms in the Cu first coordination sphere.

Even if in the PPI-G4 case the Cu coordination geometry is distorted compared to the most stable square-planar Cu^{2+} coordination, the distortion is due to the activation of water molecules by basic nitrogen atoms in the nearby of the Cu-

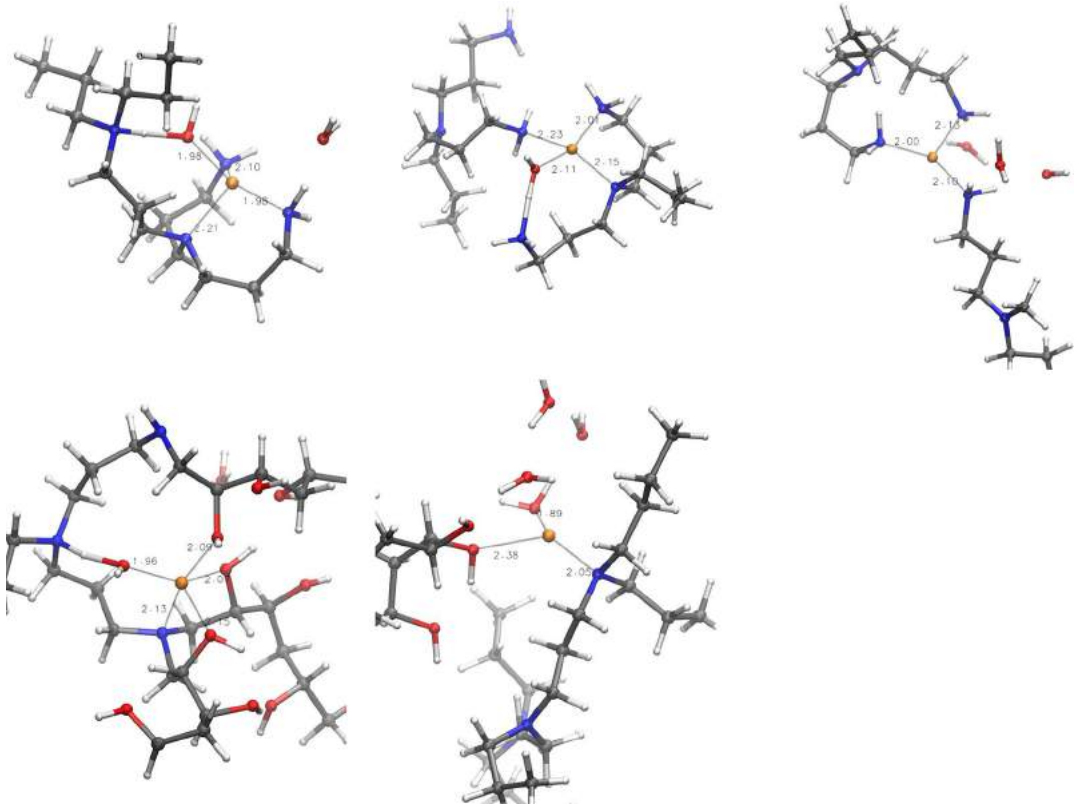

Figure 6. Minimal energy configurations obtained by low-temperature CP-MD of DFT models, obtained by truncation of final configurations in the MD trajectories of empirical models, with a few water solvent molcules included. Atomic and bond radii are arbitrary. The Cu atom is represented as an orange sphere, N is in blue, H in white, O in red, and C in gray. The VMD program has been used for all the molecular drawings. Top: PPI-G4, trajectories 0, 1, and 2. Bottom: PPI-G4-mal, trajectories 0 and 4.

bound water molecule. For instance, in Figure 6, top-left panel, the water molecule *anti* to the tertiary amino group is released while that *anti* to the primary amine is kept. This latter water molecule is strongly activated by the closest basic tertiary amino group, that extracts one proton from the Cu-bound water, this latter becoming an hydroxyl ion. Since the trigonal CuN_3 coordination is kept in all the PPI-G4 configurations analyzed (top panels of Figure 6), the formation of a square-planar CuN_3O geometry involving the O atom of a water molecule is easy, also because of the high solvation of the terminal amino groups (G3 and G4) in the PPI-G4 case (as shown by $g(r)$ of N(G3/G4) atoms, data not shown here).

In order to check if the exchange of proton between the Cu-bound water molecule and the tertiary amino group be an artifact of the simulation in the vacuum, a short CP-MD simulation (240 fs) was performed at T = 300 K for configuration obtained by trajectory 0 in a small sample of 152 explicit water molecules. This latter simulation shows the same proton exchange. Despite a longer simulation be necessary to eventually recover the proton by the Cu-bound water molecule, the occurrence of proton exchange denotes a contribution to the stabilization of the **N**···water−Cu alignment. This latter is possible when a few water molecules can penetrate in the region occupied by Cu and the tertiary amino groups.

The polymorphism of Cu coordination in PPI-G4-mal is larger, compared to the nondecorated PPI-G4 case, as it is shown in Figure 2, bottom-right panel. In Figure 6, bottom panels, two extreme cases are displayed. When Cu is close to terminal amino groups (in the PPI-G4-mal case these groups are bound to reduced maltose fragments), the crowding of hydroxyl groups of the reduced maltose fragment is high (see Figure 6, bottom-left). In this conditions, the coordination number reaches values of 5, with 3 hydroxyl groups, 1 tertiary amine group and one activated water molecule involved in Cu coordination. The propensity of the hydroxyl group to bind Cu, combined with the plasticity of the orientation of hydroxyl groups within the dendrimer macromolecule, disposes the coordination site to a nonplanar Cu coordination geometry. When Cu is close to the dendrimer core (a condition that is never observed in the models with no maltose decoration), the number of hydroxyl groups is smaller (see Figure 6, bottom-right). On the other hand, the number of water molecules close to the Cu-bound tertiary amino group is large. (as shown by $g(r)$ of pairs involving core atoms and O(wat) for PPI-G4-mal, Figure 4). In these conditions, a $CuNO_3$ coordination adapted to a square-planar geometry appears more likely, involving at least two water molecules available nearby to the dendrimer core.

EPR Experiments and Comparison with Computational Models. The results obtained from the modeling studies were complemented by using the computer aided EPR analysis of the Cu(II)-dendrimer solutions. Since we also wanted to obtain more information about the Cu(II)-dendrimer complexation, we performed an accurate study of the complexation behavior at increasing Cu(II) concentrations, keeping constant the dendrimer concentration in terms of external surface groups (0.1 M). However, we also performed EPR experiments at fixed Cu(II) concentration and variable dendrimer concentration. We verified that the significant

dx.doi.org/10.1021/jp505420s | J. Phys. Chem. B 2014, 118, 12098−12111

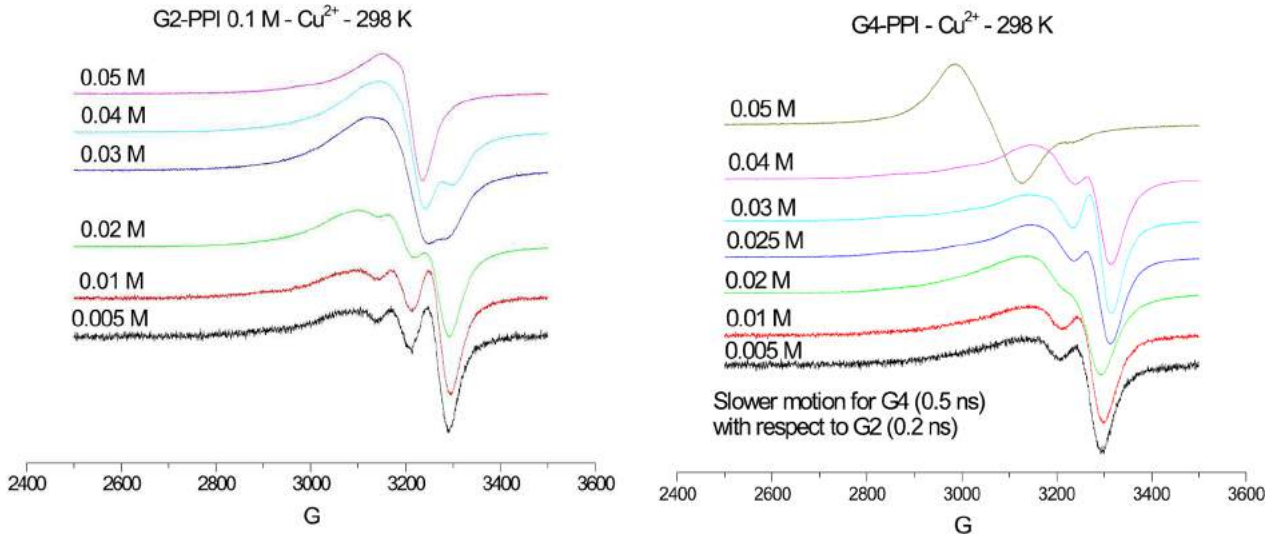

Figure 7. EPR experimental spectra (T = 298 K) obtained for 0.1 M solutions of PPI-G2 (left panel) and PPI-G4 (right panel) at selected Cu (II) concentrations.

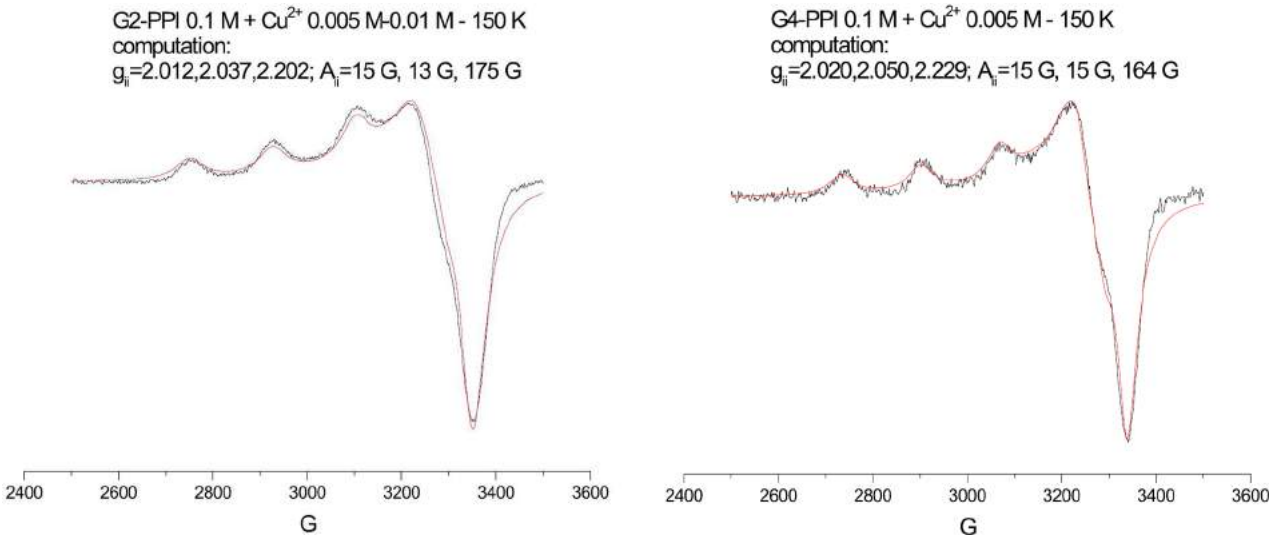

Figure 8. Experimental and computed EPR spectra of PPI-G2 (left panel) and PPI-G4 (right panel) at T = 150 K and Cu(II) concentration of 0.005 M (for PPI-G2, the spectrum is almost invariant up to 0.01 M, while, at this Cu(II) concentration, the spectrum of PPI-G4 becomes similar to that of PPI-G2). The main computation parameters are reported in the figures.

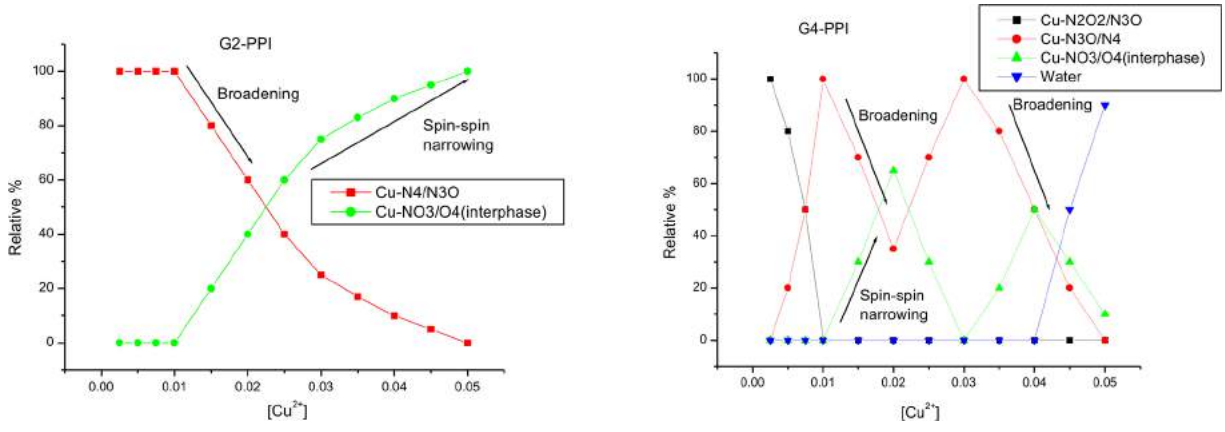

Figure 9. Contribution (%) of different computed spectra to EPR signals (Figure 7), as a function of Cu(II) concentration: PPI-G2 (left panel) and PPI-G4 (right panel).

dx.doi.org/10.1021/jp505420s | J. Phys. Chem. B 2014, 118, 12098−12111

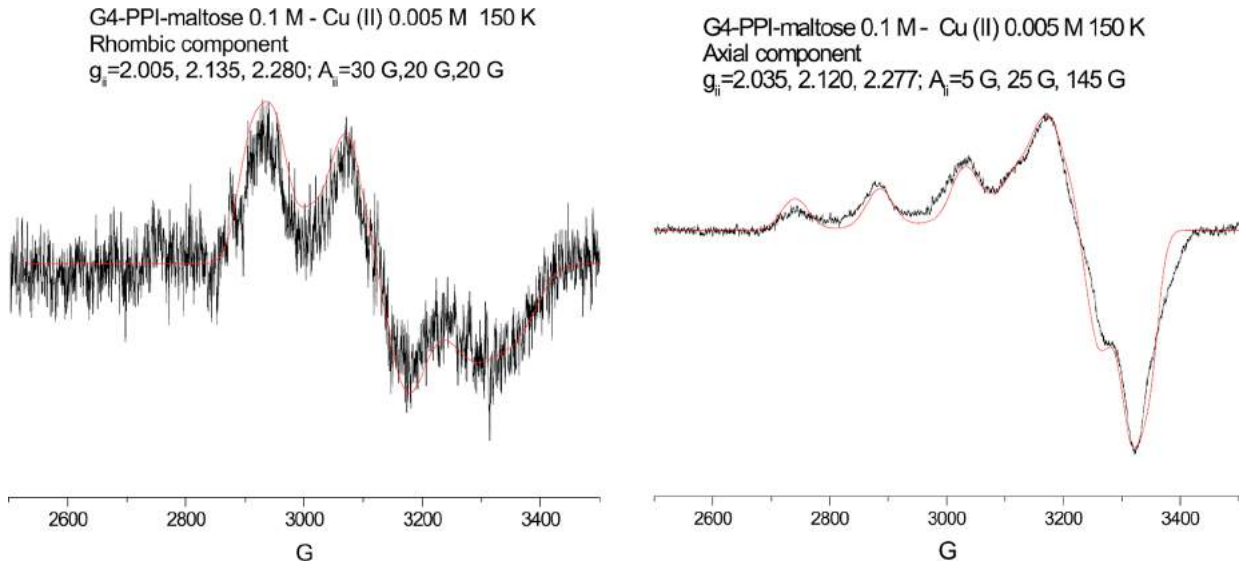

Figure 10. Computation of the rhombic (left panel) and axial (right panel) components of the spectrum of PPI-G4-mal (0.1 M) with Cu(II) concentration of 0.005 M (similar spectrum at 0.0025 M). The main parameters of computation are shown in the figure.

parameter is the molar ratio between the external dendrimer groups and the Cu(II) ions.

Figure 7 shows the EPR spectra (T = 298 K, normalized in height) obtained for 0.1 M solutions of PPI-G2 (left panel) and PPI-G4 (right panel) at selected Cu(II) concentrations. In Figure 8, the experimental and computed EPR spectra of PPI-G2 (left panel) and PPI-G4 (right panel) at T = 150 K and Cu(II) concentration of 0.005 M are shown as examples. The EPR results are nicely supported (and, in turn, support them) by the computational models. First, we clearly see from the spectra shown in Figures 7 and 8 that PPI-G2 and PPI-G4 behave in a different way.

PPI-G2. For PPI-G2 the spectra are invariant up to a concentration of 0.01 M. The invariant EPR signal of PPI-G2 is computed by using magnetic parameters which are characteristic of a square-planar $Cu-N_4$ or $Cu-N_3O$ coordination, that is a coordination with 4 nitrogen sites or 3 nitrogen and one oxygen sites. This is in line with the models described above.

Further information comes from the computation of the spectrum at room temperature, which uses the same magnetic parameters (g_{ii} and A_{ii}) as the computation of the low temperature spectrum, but it also provides the correlation time τ = 0.2 ns, characteristic of a fast motion due to the high flexibility of the low generation dendrimer.

By further increasing Cu(II) concentration, a second signal is recognized (Figure 7, left panel), whose features indicate a $Cu-NO_3/Cu-O_4$ coordination. This latter coordination is localized at the dendrimer/water interface. The relative intensity of the $Cu-NO_3/Cu-O_4$ component increases at the expenses of the $Cu-N_4/Cu-N_3O$ component as shown in Figure 9 (left panel). The $Cu-N_4/Cu-N_3O$ component is broadening due to the proximity of other Cu(II) ions. The complex at the interface decreases its line width at the highest Cu(II) concentrations due to strong spin−spin interactions in the fluid medium.

PPI-G4. For PPI-G4 at the lowest Cu(II) concentration (Figure 7, right panel) the spectrum is characteristic of a square-planar $Cu-N_2O_2/Cu-N_3O$ coordination, which is also in agreement with the results obtained with computational models. The structure of PPI-G4 reduces the chance for a low energy coordination with 4 nitrogen sites, because of the entanglement of the branches. In line with this finding, the mobility of the complex (τ = 0.5 ns) is significantly reduced because the branch flexibility around Cu is lower.

By increasing Cu(II) concentration from 0.005 to 0.01 M, the preferential $Cu-N_2O_2$ coordination is easily saturated and more nitrogen sites become available inside the dendrimer, giving rise to a $Cu-N_3O/Cu-N_4$ coordination, as shown in Figure 9 (right panel). So, for PPI-G4 the Cu(II) ions find more nitrogen rich sites at a higher concentration with respect to PPI-G2. However, Figure 9, right panel, shows that the $Cu-N_3O/N_4$ coordination of PPI-G4 undergoes to a strange behavior by further increasing Cu(II) concentration: first, a line broadening indicates the saturation of these sites and the $Cu-NO_3/Cu-O_4$ coordination at the interface appears. But, between 0.01 and 0.02 M of Cu(II) this latter component undergoes to a spin−spin narrowing since the ions concentrate in a small interfacial space. When the interface component disappears due to the very strong spin−spin interactions, the $Cu-N_3O/Cu-N_4$ reappears, since its competitor in the relative percentage to the spectrum is no more EPR visible. Then, another region of the interface gets populated while, again, the $Cu-N_3O/Cu-N_4$ saturates. Finally, also this second interface region saturates in between 0.04 and 0.05 M of Cu(II) and, above 0.04 M, the ions are definitely extruded from the dendrimer surface and are ejected from the dendrimer to the bulk water. Therefore, the EPR analysis allows us to identify different regions and structures of the dendrimer and of the complexes formed between the dendrimer and Cu(II).

PPI-G2-mal. The maltose decoration significantly changed the Cu(II) coordination behavior as shown by the modeling study which evidenced variations in the coordination structures. The EPR analysis of PPI-Gn dendrimers with maltose decoration in the presence of Cu(II) has been already discussed in a previous study at Cu(II) concentrations ≥0.01 M.[9] At 0.01 M concentration it has been found for PPI-G2-mal that the structure of the complex is square-planar, but the maltose decoration prevents the ions to coordinate four nitrogen atoms and the $Cu-N_2O_2$ coordination becomes more probable, with the oxygen sites probably belonging to the OH groups of

dx.doi.org/10.1021/jp505420s | J. Phys. Chem. B 2014, 118, 12098−12111

maltose. In the present study, for a matter of comparison with the amino-decorated dendrimers and the modeling studies, we used lower Cu(II) concentrations (0.0025−0.005 M) of Cu(II). In this Cu(II) concentration range, PPI-G2-mal gave an EPR spectrum which is similar to that found for PPI-G4 (i.e., without maltose) at 0.005 M and shown in Figure 7, right panel. This indicates a $Cu-N_3O$ coordination, in perfect agreement with the most likely configuration obtained with computational models.

PPI-G4-mal. The situation for PPI-G4-mal is again more complicated. In ref 9 we found at Cu(II) concentration of 0.01 M that the ions partially (about 20%) coordinate the dendrimer sites in a nonplanar structure (rhombic) with 5 coordinating sites which were mostly identified as oxygen sites, but also a $Cu-N_2O_3$ coordination was identified (g_{ii} = 2.005, 2.135, 2.280; A_{ii} = 35, 25, 20 G). In the present study, at the lower Cu(II) concentrations (0.0025−0.005 M) of Cu(II), the rhombic coordination is more evident (about 60%), superimposed to an axial coordination (40%). The two components, extracted by subtracting one experimental spectrum from the other at close Cu(II) concentrations, were simulated as shown in Figure 10: rhombic (left panel) and axial (right panel). Interestingly, both the rhombic and the axial components show magnetic parameters consistent with $Cu-NO_4$ (rhombic) and $Cu-NO_3$ (axial) coordinations. This is again in nice agreement with the computational models.

CONCLUSION

In this work we built several computational models for a single Cu ion bound to four different PPI models: generation 2 and 4 of PPI, without and with a full maltose functionalization of terminal amino groups. The high pH (low charge) states have been simulated within an empirical force-field and several final configurations have been truncated and modeled at the level of density-functional theory for better representing electronic effects in the Cu coordination.

The results of these models show that the change in Cu binding when the maltose decoration is added to PPI-Gn in complex with copper, is dominated by the interactions within maltose units. The Cu ion is displaced by the most likely N-terminal coordination in PPI-G4 because of the hindering of N terminal atoms due to the many hydroxyl groups of the reduced maltose fragment that bind Cu in that region. This effect is stronger in PPI-G4 than in PPI-G2, where the N−Cu bonds are indeed less affected.

EPR spectra recorded for the same species at variable Cu concentration, including low values, display the same drastic change for Cu coordination when the maltose decoration is present in PPI-G4. This effect is particularly evident for low Cu concentration, that is at the working conditions for PPI-mal in biological fluids.

Both simulations and EPR spectra reveal a mechanism by which Cu ions are displaced by the N-termini, these latter opened by their maltose decoration, and move toward the closer available binding sites. In models, only in a few cases the Cu ion is bound to one of the low-density N atoms in the dendrimer core, where, in PPI-G4, the many water molecules that are kept around the dendrimer by the maltose decoration can easily fill the free valences of Cu. These latter Cu-binding sites, of type NO_3, may adopt more easily a square-planar geometry compared to those sites close to N(G4) and maltose decoration. In these latter cases, the crowding of available hydroxyl groups enhance the rhombic distortion of the Cu coordination.

The results of this study indicate a possible effect on copper chemistry due to the different type of Cu-dendrimer interactions when maltose is introduced. Since maltose decoration is an essential modification for dendrimer usage in biological fluids, it is of utmost importance to predict possible chemical consequences of this modification.

The models reported in this work are starting points to set up more complex models, where the modulation of long-range interactions due to metal ions in competition with protons can be encoded in the initial constructions based on Monte Carlo random walks including different schemes for random insertion of ions. These improvements are mandatory for exploiting the copper binding at lower pH, closer to physiological conditions. In these conditions the competition of dendrimers with other Cu-binding macromolecules, like amyloid β peptides and α-synuclein, is an important effect to take into account.

AUTHOR INFORMATION

Corresponding Authors

*E-mail: maria.ottaviani@uniurb.it.
*E-mail: andrea.danani@supsi.ch.

Notes

The authors declare no competing financial interest.

ACKNOWLEDGMENTS

This work has been done within the project "Molecular modelling of dendrimers-polypeptide fibril interactions for neurodegenerative diseases therapies" (POLYDEN-COST C10.0146) supported by Swiss State Secretariat for Education, Research and Innovation (SERI). The authors are grateful to Dr. Marco Deriu for useful comments.

REFERENCES

(1) Faller, P.; Hureau, C. Preface to the Special Issue: Metal Ions in Neurodegenerative Diseases. *Coord. Chem. Rev.* **2012**, *256*, 2127−2128.

(2) Halliwell, B. Oxidative Stress and Neurodegeneration: Where Are We Now? *J. Neurochem.* **2006**, *97*, 1634−1658.

(3) La Penna, G.; Hureau, C.; Andreussi, O.; Peter, F. Identifying, by First-Principles Simulations, Cu[Amyloid-β] Species Making Fenton-Type Reactions in Alzheimers Disease. *J. Phys. Chem. B* **2013**, *117*, 16455−16467.

(4) Bertini, I., Gray, H. B., Stiefel, E. I., Valentine, J. S., Eds. *Biological Inorganic Chemistry: Structure and Reactivity*; University Science Books: Herndon, VA, 2007.

(5) Boll, M.-C.; Alcaraz-Zubeldia, M.; Montes, S.; Rios, C. Free Copper, Ferroxidase and SOD1 Activities, Lipid Peroxidation and NOx Content in the CSF. A Different Marker Profile in four Neurodegenerative Diseases. *Neurochem. Res.* **2008**, *33*, 1717−1723.

(6) Koizumi, M.; Fujii, J.; Suzuki, K.; Inoue, T.; Inoue, T.; Gutteridge, J. M. C.; Taniguchi, N. A Marked Increase in Free Copper Levels in the Plasma and Liver of LEC Rats: An Animal Model for Wilson Disease and Liver Cancer. *Free Radical Res.* **1998**, *28*, 441−450.

(7) Humpel, C. Identifying and Validating Biomarkers for Alzheimer's Disease. *Trends Biotechnol.* **2011**, *29*, 26−32.

(8) Bosman, A. W.; Schenning, A. P. H. J.; Janssen, R. A. J.; Meijer, E. W. Well-Defined Metal-lodendrimers by Site-Specific Complexation. *Chem. Ber.* **1997**, *130*, 725−728.

(9) Appelhans, D.; Oertel, U.; Mazzeo, R.; Komber, H.; Hoffmann, J.; Weidner, S.; Brutschy, B.; Voit, B.; Ottaviani, F. M. Dense-shell Glycodendrimers: UV/Vis and Electron Paramagnetic Resonance

Study of Metal Ion Complexation. *Proc. R. Soc. Chem.* **2010**, *466*, 1489−1513.
(10) Ottaviani, M. F.; Bossmann, S.; Turro, N. J.; Tomalia, D. A. Characterization of Starburst Dendrimers by the EPR Technique. 1. Copper Complexes in Water Solution. *J. Am. Chem. Soc.* **1994**, *116*, 661−671.
(11) Ottaviani, M. F.; Montalti, F.; Turro, N. J.; Tomalia, D. A. Characterization of Starburst Dendrimers by the EPR Technique. Copper(II) Ions Binding Full-Generation Dendrimers. *J. Phys. Chem. B* **1997**, *101*, 158−166.
(12) Ottaviani, M. F.; Valluzzi, R.; Balogh, L. Internal Structure of Silver Poly(amidoamine) Dendrimer Complexes and Nanocomposites. *Macromolecules* **2002**, *35*, 5105−5115.
(13) Galán, M.; Sánchez-Rodríguez, J.; Cangiotti, M.; Gárcia-Gallego, S.; Jiménez, J. L.; Gómez, R.; Ottaviani, M. F.; Muñoz Fernández, M. A.; Javier de la Mata, F. Antiviral Properties Against HIV of Water Soluble Copper Carbosilane Dendrimers and Their EPR Characterization. *Curr. Med. Chem.* **2012**, *19*, 4984−4994.
(14) Gárcia-Gallego, S.; Cangiotti, M.; Fiorani, L.; Fattori, A.; Muñoz Fernández, M. A.; Gómez, R.; Ottaviani, M. F.; Javier de la Mata, F. Anionic Sulfonated and Carboxylated PPI Dendrimers with the EDA Core: Synthesis and Characterization of Selective Metal Complexing Agents. *Dalton Trans.* **2013**, *42*, 5874−5889.
(15) Ottaviani, M. F.; Cangiotti, M.; Fattori, A.; Coppola, C.; Lucchi, S.; Ficker, M.; Petersen, J. F.; Christensen, J. B. Copper(II) Complexes with 4-Carbomethoxypyrrolidone Functionalized PAMAM-Dendrimers: An EPR Study. *J. Phys. Chem. B* **2013**, *117*, 14163−14172.
(16) Ottaviani, M. F.; Cangiotti, M.; Fattori, A.; Coppola, C.; Posocco, P.; Laurini, E.; Liu, X.; Liu, C.; Fermeglia, M.; Peng, L.; et al. Copper(ii) Binding to Flexible Triethanolamine-Core PAMAM Dendrimers: A Combined Experimental/In Silico Approach. *Phys. Chem. Chem. Phys.* **2014**, *16*, 685−694.
(17) Ziemba, B.; Franiak-Pietryga, I.; Pion, M.; Appelhans, D.; Munoz-Fernandez, M. A.; Voit, B.; Bryszewska, M.; Klajnert-Maculewicz, B. Toxicity and Proapoptotic Activity of Poly(propylene imine) Glycodendrimers In Vitro: Considering their Contrary Potential as Biocompatible Entity and Drug Molecule in Cancer. *Int. J. Pharm.* **2014**, *461*, 391−402.
(18) Tian, W.-d.; Ma, Y.-q. Theoretical and Computational Studies of Dendrimers as Delivery Vectors. *Chem. Soc. Rev.* **2013**, *42*, 705−727.
(19) Naylor, A. M.; Goddard, W.; Kieffer, G.; Tomalia, D. Starbust Dendrimers. Molecular Shape Control. *J. Am. Chem. Soc.* **1989**, *111*, 2339−2341.
(20) Mansfield, M. L.; Klushin, L. I. Monte Carlo Studies of Dendrimer Macromolecules. *Macromolecules* **1993**, *26*, 4262−4268.
(21) Han, M.; Chen, P.; Yang, X. Molecular Dynamics Simulation of PAMAM Dendrimer in Acqueous Solution. *Polymer* **3488**, *46*, 3481.
(22) Maiti, P.; Cagin, T.; Lin, S.; Goddard, W. Effect of Solvent and pH on the Structure of PAMAM Dendrimers. *Macromolecules* **2005**, *38*, 979−991.
(23) Lin, S.; Maiti, P.; Goddard, W. Dynamics and Thermodynamics of Water in PAMAM Dendrimers at Subnanosecond Time Scales. *J. Phys. Chem. B* **2005**, *109*, 8663−8672.
(24) Carbone, P.; Müller-Plathe, F. Molecular Dynamics Simulations of Polyaminoamide (PAMAM) Dendrimer Aggregates: Molecular Shape, Hydrogen Bonds and Local Dynamics. *Soft Matter* **2009**, *5*, 2638−2647.
(25) Jensen, L.; Pavan, G.; M. Kasimova, M.; Rutherford, S.; Danani, A.; Nielsen, H. M.; Foged, C. Elucidating the Molecular Mechanism of PAMAM-siRNA Dendriplex Selfassembly: Effect of Dendrimer Charge Density. *Int. J. Pharm.* **2011**, *416*, 410−418.
(26) Freire, J.; Ahmadi, A.; McBride, C. Molecular Dynamics Simulations of the Protonated G4 PAMAM Dendrimer in an Ionic Liquid System. *J. Phys. Chem. B* **2013**, *117*, 15157−15164.
(27) Pavan, G. M.; Barducci, A.; Albertazzi, L.; Parrinello, M. Combining Metadynamics Simulation and Experiments to Characterize Dendrimers in Solution. *Soft Matter* **2013**, *9*, 2593−2597.
(28) Jayamurugan, C.; Ganapathy, R.; Maiti, P.; Jayaraman, N.; Sood, A. Structure of Poly(propyl ether imine) Dendrimer from Fully Atomistic Molecular Dynamics Simulation and by Small Angle X-ray Scattering. *J. Chem. Phys.* **2006**, *124*, 204719−204730.
(29) Tanis, I.; Karatasos, K. pH Response of Conformation of Poly(propylene imine) Dendrimer in Water: a Molecular Simulation Study. *Phys. Chem. Chem. Phys.* **2009**, *11*, 10017−28.
(30) Wua, C. pH Response of Conformation of Poly(propylene imine) Dendrimer in Water: a Molecular Simulation Study. *Mol. Sim.* **2010**, *36*, 1164−1172.
(31) McCarthy, J.; Rasines Moreno, B.; Filippini, D.; Komber, H.; Maly, M.; Cernescu, M.; Brutschy, B.; Appelhans, D.; Rogers, M. Influence of Surface Groups on Poly(propylene imine) Dendrimers Anti-Prion Activity. *Biomacromolecules* **2013**, *14*, 27−37.
(32) Maly, J.; Pedziwiatr-Werbicka, E.; Maly, M.; Semeradtova, A.; Appelhans, D.; Danani, A.; Zaborski, M.; Klajnert, B.; Bryszewska, M. Highly Organized Self-Assembled Dendriplexes Based on Poly(propylene imine) Glycodendrimer and Anti-HIV Oligodeoxynucleotides. *Curr. Med. Chem.* **2012**, *19*, 4708−4719.
(33) Garzoni, M.; Cheval, N.; Fahmi, A.; Danani, A.; Pavan, G. M. Ion-Selective Controlled Assembly of Dendrimer-Based Functional Nanofibers and their Ionic-competitive Disassembly. *J. Am. Chem. Soc.* **2012**, *134*, 3349−3357.
(34) Pang, Y.-P.; Xu, K.; El Yazal, J.; Prendergast, F. G. Successful Molecular Dynamics Simulation of the Zinc-Bound Farnesyltransferase Using the Cationic Dummy Atom Approach. *Protein Sci.* **2000**, *9*, 1857−1865.
(35) Furlan, S.; Hureau, C.; Faller, P.; La Penna, G. Modeling the Cu^+ Binding in the 1−16 Region of the Amyloid-β Peptide Involved in Alzheimer's Disease. *J. Phys. Chem. B* **2010**, *114*, 15119−15133.
(36) Cornell, W. D.; Cieplak, P.; Bayly, C. I.; Gould, I. R.; Merz, K. M. J.; Ferguson, D. M.; Spellmeyer, D. C.; Fox, T.; Caldwell, J. W.; Kollman, P. A. A Second Generation Force Field for the Simulation of Proteins, Nucleic Acids, and Organic Molecules. *J. Am. Chem. Soc.* **1995**, *117*, 5179−5197.
(37) Jorgensen, W. L.; Chandrasekhar, J.; Madura, J. D.; Impey, R. W.; Klein, M. J. Comparison of Simple Potential Functions for Simulating Liquid Water. *J. Chem. Phys.* **1983**, *79*, 926−935.
(38) Guvench, O.; Mallajosyula, S. S.; Raman, E. P.; Hatcher, E. R.; Vanommeslaeghe, K.; Foster, T. J.; Jamison, F. W.; MacKerell, A. D., Jr. CHARMM Additive All-Atom Force Field for Carbohydrate Derivatives and its Utility in Polysaccharide and Carbohydrate-Protein Modeling. *J. Chem. Theory Comput.* **2011**, *7*, 3162−3180.
(39) La Penna, G.; Morante, S.; Perico, A.; Rossi, G. C. Designing Generalized Statistical Ensembles for Numerical Simulations of Biopolymers. *J. Chem. Phys.* **2004**, *121*, 10725−10741.
(40) Furlan, S.; La Penna, G.; Perico, A. Modeling the Free Energy of Polypeptides in Different Environments. *Macromolecules* **2008**, *41*, 2938−2948.
(41) Barducci, A.; Chelli, R.; Procacci, P.; Schettino, V.; Gervasio, F. L.; Parrinello, M. Metadynamics Simulation of Prion Protein: β-Structure Stability and the Early Stages of Misfolding. *J. Am. Chem. Soc.* **2006**, *128*, 2705−2710.
(42) Essmann, U.; Perera, L.; Berkowitz, M. L.; Darden, T.; Lee, H.; Pedersen, L. G. A Smooth Particle Mesh Ewald Method. *J. Chem. Phys.* **1995**, *103*, 8577−8593.
(43) Phillips, J. C.; Braun, R.; Wang, W.; Gumbart, J.; Tajkhorshid, E.; Villa, E.; Chipot, C.; Skeel, R. D.; Kalé, L.; Schulten, K. Scalable Molecular Dynamics with NAMD. *J. Comput. Chem.* **2005**, *26*, 1781−1802, http://www.ks.uiuc.edu/Research/namd.
(44) Andersen, H. C. RATTLE: A Velocity Version of the SHAKE Algorithm for Molecular Dynamics. *J. Comput. Phys.* **1983**, *52*, 24−34.
(45) Berendsen, H. J. C.; Postma, J. P. M.; Van Gunsteren, W. F.; Di Nola, A.; Haak, J. R. Molecular Dynamics with Coupling to an External Bath. *J. Chem. Phys.* **1984**, *81*, 3684−3690.
(46) Scherrenberg, R.; Coussens, B.; van Vliet, P.; Edouard, G.; Brackman, J.; de Brabander, E.; Mortensen, K. The Molecular Characteristics of Poly(propyleneimine) Dendrimers As Studied with Small-Angle Neutron Scattering, Viscosimetry, and Molecular Dynamics. *Macromolecules* **1998**, *31*, 456−461.

(47) Car, R.; Parrinello, M. Unified Approach for Molecular Dynamics and Density-Functional Theory. *Phys. Rev. Lett.* **1985**, *55*, 2471−2474.
(48) Marx, D.; Hutter, J. *Ab Initio Molecular Dynamics: Basic Theory and Advanced Methods*; Cambridge University Press: Cambridge, 2009.
(49) Giannozzi, P.; Baroni, S.; Bonini, N.; Calandra, M.; Car, R.; Cavazzoni, C.; Ceresoli, D.; Chiarotti, G. L.; Cococcioni, M.; Dabo, I.; et al. QUANTUM ESPRESSO: A Modular and Open-Source Software Project for Quantum Simulations of Materials. *J. Phys.: Condens. Matter* **2009**, *21*, 395502 http://www.quantum-espresso.org.
(50) Vanderbilt, D. Soft Self-Consistent Pseudopotentials in a Generalized Eigenvalue Formalism. *Phys. Rev. B* **1990**, *41*, 7892−7895.
(51) Perdew, J. P.; Burke, K.; Ernzerhof, M. Generalized Gradient Approximation Made Simple. *Phys. Rev. Lett.* **1996**, *77*, 3865−3868.
(52) Nosé, S. A Molecular Dynamics Method for Simulations in the Canonical Ensemble. *Mol. Phys.* **1984**, *52*, 255−268.
(53) Frenkel, D.; Smit, B. *Understanding Molecular Simulation*; Academic Press: San Diego, U.S.A., 1996.
(54) Appelhans, D.; Zhong, Y.; Komber, H.; Friedel, P.; Oertel, U.; Scheler, U.; Morgner, N.; Kuckling, D.; Richter, S.; Seidel, J.; et al. Oligosaccharide-Modified Poly(propyleneimine) Dendrimers: Synthesis, Structure Determination, and Cu(II) Complexation. *Macromol. Biosci.* **2007**, *7*, 373−383.
(55) Budil, D. E.; Lee, S.; Saxena, S.; Freed, J. H. Nonlinear-Least-Squares Analysis of Slow-Motion EPR Spectra in One and Two Dimensions Using a Modified LevenbergMarquardt Algorithm. *J. Magn. Res., Ser. A* **1996**, *120*, 155−189.
(56) Hathaway, B.; Tomlinson, A. A. G. Copper(II) Ammonia Complexes. *Coord. Chem. Rev.* **1970**, *5*, 1−43.
(57) Peisach, J.; Blumberg, W. E. Structural Implications Derived from the Analysis of Electron Paramagnetic Resonance Spectra of Natural and Artificial Copper Proteins. *Arch. Biochem. Biophys.* **1974**, *165*, 691−708.
(58) Addison, A. W. Spectroscopic and Redox Trends from Model Copper Complexes. In *Copper Coordination Chemistry: Bio-Chemical and Inorganic Perspectives*; Karlin, K. D., Zubieta, J., Eds.; Adenine Press: Guilderland, NY, 1983; pp 109−115.
(59) Gampp, H. Investigation of Complex Equilibria in Solution by EPR Spectroscopy. *Inorg. Chem.* **1984**, *23*, 1553−1557.
(60) Basosi, R.; Della Lunga, G.; Pogni, R. Biological Magnetic Resonance. In *Biomedical EPR, Part A: Free Radicals, Metals, Medicine, and Physiology*; Eaton, S. R., Eaton, G. R., Berliner, L. J., Eds.; Springer: New York, 2005; Vol. *23*; pp 385−416.
(61) Solomon, E. I.; Hanson, M. A. In *Inorganic Electronic Structure and Spectroscopy, Vol. II: Applications and Case Studies*; Solomon, E. I., Lever, E. A. B. P., Eds.; John Wiley & Sons: New York, 2006; Chapter Bioinorganic Spectroscopy, pp 1−130.
(62) Theodorou, D. N.; Suter, U. W. Shape of Unperturbed Linear Polymers: Polypropylene. *Macromolecules* **1985**, *18*, 1206−1214.
(63) Shental-Bechor, D.; Levy, Y. Effect of Glycosylation on Protein Folding: A Close Look at Thermodynamic Stabilization. *Proc. Natl. Acad. Sci. U.S.A.* **2008**, *105*, 8256−8261.